IEEE Photonics Journal
An IEEE Photonics Society Publication

Open Access

Two-Segment Gain-Coupled Distributed Feedback Laser

Volume 10, Number 1, February 2018

Feng Gao
Li Qin
Yong-Yi Chen
Peng Jia
Chao Chen
Hong Chen
Lei Liang
Yu-Gang Zeng
Xing Zhang
Yong-Qiang Ning
Ye-Jin Zhang
Li-Jun Wang

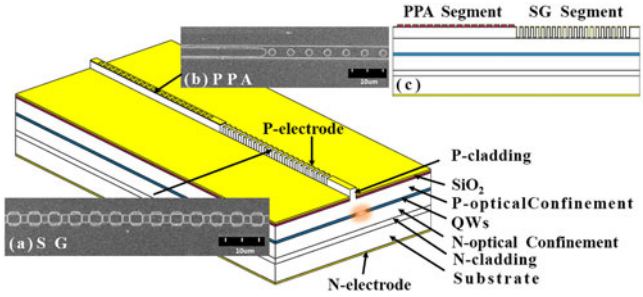

DOI: 10.1109/JPHOT.2018.2791610
1943-0655 © 2018 IEEE

IEEE photonics SOCIETY

IEEE

Two-Segment Gain-Coupled Distributed Feedback Laser

Feng Gao,[1,2] **Li Qin**,[1] **Yong-Yi Chen**,[1] **Peng Jia**,[1] **Chao Chen**,[1] **Hong Chen**,[1,2] **Lei Liang**,[1] **Yu-Gang Zeng**,[1] **Xing Zhang**,[1] **Yong-Qiang Ning**,[1] **Ye-Jin Zhang**,[3] **and Li-Jun Wang**[1]

[1]State Key Laboratory of Luminescence and Application, Changchun Institute of Optics, Fine Mechanics and Physics, Chinese Academy of Sciences, Changchun 130033, China
[2]University of Chinese Academy of Sciences, Beijing 100049, China
[3]Institute of Semiconductors, Chinese Academy of Sciences, Beijing 100083, China

DOI:10.1109/JPHOT.2018.2791610

Manuscript received November 7, 2017; revised January 1, 2018; accepted January 7, 2018. Date of publication January 10, 2018; date of current version January 23, 2018. This work is supported in part by the National Science and Technology Major Project of China under Grant 2016YFE0126800, in part by the Frontier Science Key Program of President of the Chinese Academy of Sciences (QYZDY-SSW-JSC006), in part by the National Natural Science Foundation of China under Grants 61234004, 51672264, 61674148, 11604328, 11404327, 61505206, and 61235004, and in part by the Natural Science Foundation of Jilin Province (Jilin Province Natural Science Foundation) (20160520017JH, 20170623024TC, 20150520089JH, 20150203007GX, 20150204042GX, and 20160414016GH). Corresponding authors: Li Qin and Yong-Yi Chen (e-mail: qinl@ciomp.ac.cn; chenyy@ciomp.ac.cn).

Abstract: A two-segment regrowth-free gain-coupled distributed feedback (DFB) laser monolithically integrated different gain contrast segments was proposed, realizing both wavelength-tunable (5 nm) and wavelength stabilization characteristics, controlled by a single electrode only. At current larger than 320 mA, side mode suppression ratio reached $>$30 dB with 3 dB linewidth $<$80 pm. The CW power reached up to 159 mW/facet at single-mode operation. Considering both uncoated facets all together, it is at the same power level as index-coupled DFB lasers. Periodic surface grooves and 4-μm-width ridge were patterned merely by one-step i-line lithography. It provides a novel method for low-cost practical gain-coupled DFB laser fabrication, which can be used in either/both wavelength-tunable applications such as sensing and detection, or/and wavelength stabilization fields such as pumping fiber lasers.

Index Terms: Semiconductor lasers, distributed-feedback, single-mode, tunable lasers.

1. Introduction

Distributed feedback (DFB) lasers have become essential single-mode light sources in spectroscopy [1] and pumping sources [2]. On one hand, DFB lasers with tunable single longitudinal mode and narrow linewidth not only fit various working wavelengths but also ensure efficiency of detection. Thus, they have a wide application field: from tunable LIDAR [3] used in robots, 3D sensing and intelligent driving to differential absorption LIDAR [4] (e.g., tracking specific gas with spectral absorption linewidth). Multi-sectional index-coupled DFB lasers with separated electrodes can effectively enhance wavelength tuning range [5]–[10]. However, two or more Bragg modes in the same cavity tend to compete against each other, resulting in a fast degradation of SMSR or mode-hopping. Meanwhile complicated, precise and tedious control of injection current is required [11], causing them difficult to maintain a long-term stable operation. Separated top contacts (three-terminal

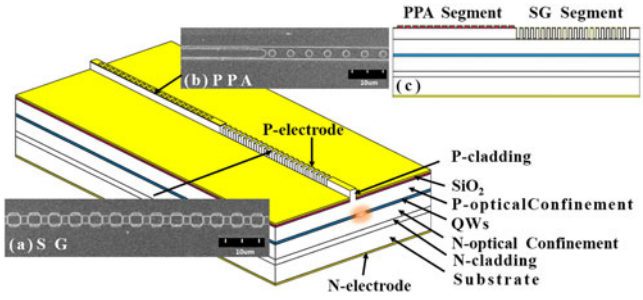

Fig. 1. Device Schematic. (a) Scanning electron microscope image for the top of SG segment, (b) SEM for the top of PPA segment, (c) Cross-section.

configuration) also require complex fabrication and package steps, and cause the instability from the changes of separation between different segments with the variation of temperature.

On the other hand, wavelength stabilization is another key issue for DFB lasers, especially when DFB lasers are used for pumping Er-doped fiber amplifiers (EDFAs) [12] or fiber optic gyroscope. Heat accumulation or current changing in common DFB lasers [13], [14] could cause pumping wavelength shift and greatly reduce pumping efficiency. Even though a number of structures have been proposed to stabilize wavelength [15]–[17], external modulations are required including the addition of absolute wavelength references, polarization-independent heterodyne detectors, control electronics, interconnections and FP etalons, significantly increasing the complexity and the space.

In this paper, a monolithically integrated regrowth-free gain-coupled DFB laser with two segments of equal length and same-period electrode as same P-contact is proposed. Our device realizes enhanced wavelength-tuning range and wavelength stabilization simultaneously controlled by only one electrode. To our best knowledge, it's the first time that gain-coupled DFB lasers possess both characteristics above. The control of current distribution implies a limited control of carrier density distribution along the laser cavity. And with the change of carrier density, gain peak could change [18]. Indeed, these mechanisms are believed to be responsible for assuring both continuous tuning and frequency switching [19]–[21]. What's more, gain-coupled DFB lasers with surface periodic current injection requiring only i-line lithography, is much easier to be fabricated without expensive and time-consuming fabrication steps such as nanoscale grating fabrication, second epitaxy or high quality anti-reflection facet coating technology. The implementation of gain-coupled effect can effectively remove mode degeneracy to realize single-longitudinal-mode operation without facet coatings technology [22], [23], benefitting from facet immunity [24], high single-longitudinal-mode yield [25], and less sensitive to external feedback [26]. The same P-contact reduces complex sealing steps, easily maintaining stable operation. With a simple and robust technique, our device benefits from an enhanced wavelength-tunable range (5 nm). For a large range of current region from 380 mA to 520 mA, the spectrum maintains stable emission wavelength (drift $<$ 0.04 nm) with SMSR over 30 dB and linewidth below 80 pm. High single mode CW output power reached up to 159 mW/facet at 580 mA at each uncoated facet. If both facets are counted, this will be a same power level as index-coupled DFB lasers [27], [28].

2. Structure and Fabrication

Device schematic is shown in Fig. 1. The 2 mm-cavity-length laser comprises two segments. One segment with 1 mm cavity length contains surface grooves (namely Surface Groove (SG) segment) and another segment with 1 mm cavity length contains purely periodic surface metal p-contact (namely Purely Periodic Anode (PPA) segment) as shown in Fig. 2. Both segments work as 44th order gain-coupled DFB lasers (6.2 μm period) with the only difference that, etched grooves (570 nm depth) enhance the contrast of carrier density in the quantum well (QW) thus increasing the contrast of gain [29], making the SG segment a better optical feedback than the PPA segment in the same length. In order to reduce index coupled effect in SG segment introduced by periodic grooves which

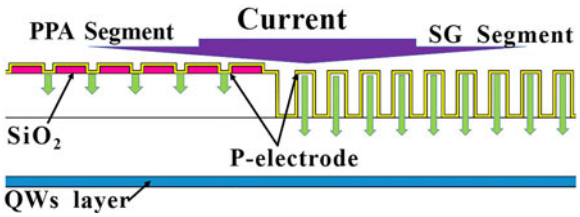

Fig. 2. Schematic of current injection operation.

TABLE 1
Epitaxial Structures for Two-Segment Gain-Coupled DFB Laser

Layer	Composition	Thickness(nm)
1 Cap	p+ : GaAs	120
2 P-optical confinement	p : AlGaAs	1700
3 QWs	GaAs&InGaAs	18
4 N-optical confinement	p : AlGaAs	3715
5 Substrate	n+ : GaAs	~350000

may cause scattering loss [30], [31], small index coupling coefficient κL is designed. The theoretical calculation for κL [32]:

$$\kappa L = \frac{L}{\Lambda}\left(\frac{\Delta n}{n_{\text{eff}}}\right) \tag{1}$$

where $L = 1$ mm represents the cavity length of SG segment. $\Lambda = 6.2\ \mu$m is the period for the $l = 44$th order grating. Δn is refractive index change in the waveguide. n_{eff} is the effective index of the gratings.

Large Λ (6.2 μm comparing with ~250 nm for index-coupled DFB lasers [33], [34]) and small Δn (changing from 3.448/unetched area to 3.447/groove, simulation result given by commercial software COMSOL Multiphysics) were chosen for our devices, leading to the calculated κL 0.0467 for the cavity length of 1 mm in SG segment. This caused a very weak index coupled effect that can be neglected (κL was greater than 1 for index-coupled DFB lasers and 0.3 for high order index Bragg gratings lasers, where lasing occurs in multiple lateral modes [35]), assuring the SG segment gain-coupled. And the emission wavelength depends on the gain-coupled gratings with feedback effect provided by a periodic change of gain both in PPA and SG segments.

The epitaxial wafer was grown by Metal Organic Chemical Vapor Deposition (MOCVD) based on asymmetrical cladding structure consisting of GaAs/InGaAs quantum well designed for an emission peak at 970 nm as shown in Table 1. Periodic grooves with a periodicity of 6.2 μm and 4 μm-width ridge were patterned simultaneously by i-line lithography and then etched to 570 nm by Inductively Coupled Plasma (ICP). Aluminum doping layer below the highly doped cap layer was exposed to the air. Then partially oxidation was carried out to make the groove structure isolation with larger resistance, leaving the top of the highly doped GaAs cap layer (unetched area) to be the only available current injection region in SG segment. Then silica layer was deposited on the top of chips by plasma enhanced chemical vapor deposition (PECVD) to make electrical insulation. I-line lithography was used again for periodic current window on both SG segment with 1-mm cavity length (as shown in Fig. 1(a)) and PPA segment with 1-mm cavity length simultaneously (as shown in Fig. 1(b)). Patterns were transferred to silica layer by ICP. And after metallization, surface periodic

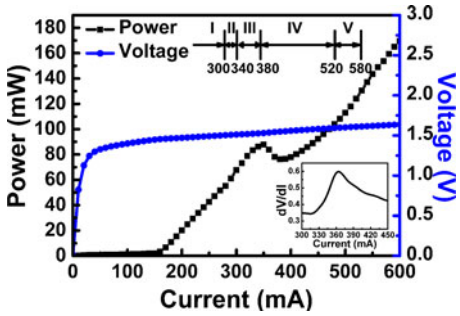

Fig. 3. CW power-voltage-current characteristics at 20 °C. The inset show dV/dI vs I characteristic.

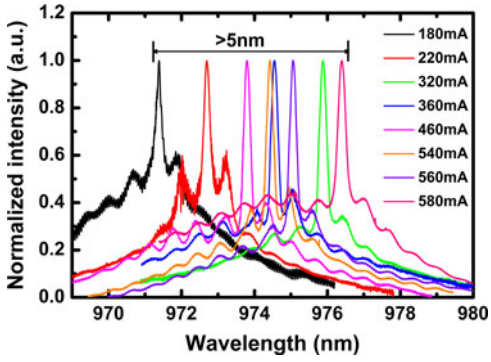

Fig. 4. CW spectrum characteristics with various currents at 20 °C.

metal p-contacts were formed in both segments, making two segments coherently connecting each other. Finally, the chips were cleaved to 2 mm cavity length without facets coating. Devices were mounted p-side down on Cu C-mount heat sinks, sharing the same anode.

3. Results and Discussion

The PIV characteristics are shown in Fig. 3. Continuous-wave (CW) test was carried out based on water-cooling unit at 20 °C. Fig. 2 shows schematically how the current was injected when the fabricated device was in test. The device has a threshold current of 160 mA. From threshold current to 320 mA, the device has a slope efficiency of 0.47 W/A, increasing the power to 86 mW at 340 mA. A clear kinking in power has been observed at current from 320 mA to 380 mA. The power drops from 87 mW to 76 mW while slope efficiency decrease to 0.35 W/A. Then the device shows a linear increase with current again, and output power increases to 159 mW when injection current reaches 580 mA. Considering both uncoated facets all together, it is at the same power level as index-coupled DFB lasers [27], [28].

CW spectrum characteristics were measured by optical fiber coupled spectrum analyzer (YOKOGAWA AQ6370C). The spectra in normalized intensity at different current levels are clearly shown in Fig. 4. Extracted information about lasing wavelength spectrum, SMSR are shown in Fig. 5. Thanks to gain-coupled effect, single longitudinal mode was achieved even without facets coating. We find that the lasing spectrum behaves exactly as the PIV characteristics. We divide the current range into five sections to describe its spectrum characteristic. Section 1: from threshold current to 300 mA, as the power increases, the device has a tuning effect: lasing wavelength increases as the current and power increases, from 971.33 nm at 180 mA to 975.24 nm at 300 mA. Spectrum behaves single longitudinal mode but SMSR is low. Section 2: from 300 mA to 340 mA, the power increases linearly, but spectrum increase a little from 975.24 nm (300 mA) to 975.88 nm (320 $\sim$ 340 mA) and kept stable, with a much higher SMSR ($>$30 dB). Section 3: from 340 mA to

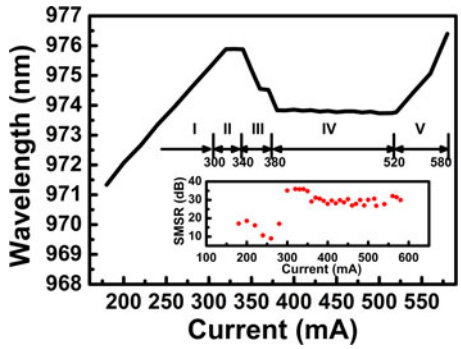

Fig. 5. Lasing wavelengths (inset: SMSR information) with various currents at 20 °C.

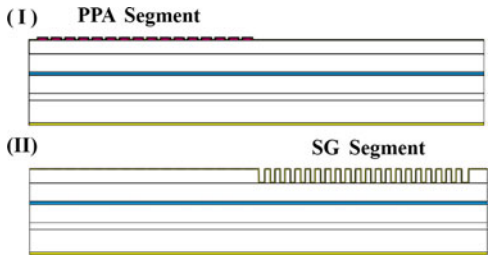

Fig. 6. Device schematic of, (I) 1-mm-length PPA segment with 1-mm-length stripe-contact segment. (II) 1-mm-length SG segment with 1-mm-length stripe-contact segment.

380 mA, the power drops from 86 mW (340 mA) to 76 mW (380 mA) and lasing spectrum blue shifts from 975.88 nm (340 mA) to 973.84 nm (380 mA), SMSR is over 30 dB. Section 4: from 380 mA to 520 mA, as power increases linearly from 76 mW (380 mA) to 123 mW (520 mA), the lasing spectrum maintains stable at 973.80 $\pm$ 0.04 nm. At a current region of 140 mA, the spectrum doesn't change larger than the equipment's system resolution (0.02 nm) and behaves a high SMSR ($\sim$30 dB) and low linewidth ($<$80 pm). Section 5: current larger than 520 mA, power increases to 159 mW and SMSR $\sim$ 30 dB, the lasing spectrum begins to tune along with current again, from 973.77 nm (520 mA) to 976.40 nm (580 mA). Device still keeps single longitudinal mode.

This device has a tuning range for 5 nm at its total operation current, which is much larger than the existing structure ($\sim$1 nm) [36] tuned also by varying the injection current only. Meanwhile, from 380 mA to 520 mA, it has an ultra-stable spectrum at around 973.80 nm. This can be explained below:

The device is designed with two gain-coupled DFB segments on purpose: the laser has two segments electrically parallel connected, a SG segment and a PPA segment. The two segments have same length of 1 mm and same period. In order to better understand the operating mechanism of our device, experimentally, the single 1-mm-length PPA segment and SG segment both with 1-mm-length stripe-contact segment was fabricated as shown in Fig. 6, to disclose the different characteristics such as PIV characteristics, resistance and spectrum. The PIV characteristics of those two devices are presented in Fig. 7, indicating the larger threshold current of single PPA segment (150 mA) than single SG segment (130 mA). And the resistance of single SG segment (6.08 Ω) is about 1.2 times larger than the single PPA segment (5.02 Ω) at 300 mA, experimentally as shown in the inset of Fig. 7. Noticing that in SG segment, due to etched grooves, part of the high doping cap layer and a small part of the aluminum doping layer were removed, making the SG segment larger electric resistance than the PPA segment. Since the different resistance of two segments electrically parallel connected, the PPA segment could enjoy more injection current. Moreover, the threshold current of the single PPA segment is lower, causing the PPA segment could be operating first. There are periodic surface grooves in SG segment to enhance gain-coupling effect without the introduction of index-coupling effect as mentioned above, the SG segment shows a larger

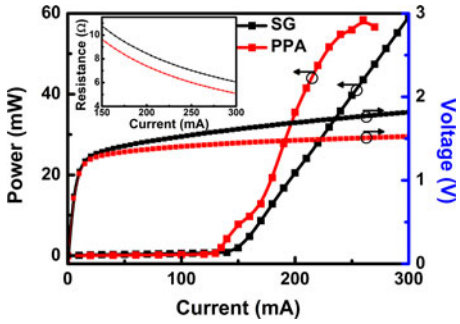

Fig. 7. CW power-voltage-current characteristics of single PPA segment and SG segment at 20 °C. The inset show the resistance vs current characteristic.

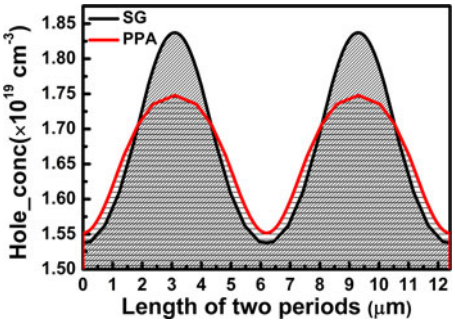

Fig. 8. The contrast of calculated one-dimensional carrier density distribution in quantum wells at 200 mA.

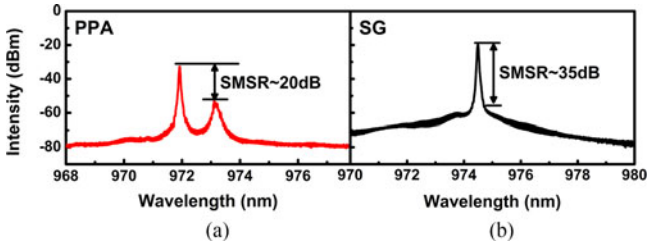

Fig. 9. CW spectrum characteristics at 200 mA at 20 °C, (a) the single PPA segment (b) the single SG segment.

contrast of carrier density. The difference of carrier density from peak to valley in SG segment is $2.99 \times 10^{18}\,cm^{-3}$, larger than $1.92 \times 10^{18}\,cm^{-3}$ of the PPA segment, calculated by the commercial software PICS3D under the current of 200 mA, as shown in Fig. 8, meaning that SG segment has a larger gain contrast and making SMSR higher than the PPA segment. To experimentally clarify the difference, the spectrum for single PPA segment and SG segment were measured at 200 mA as shown in Fig. 9. The SMSR of SG segment (35 dB) is much larger than PPA segment (20 dB). Hence, in this case, the working status of each segment can be easily discriminated from lasing spectrum, and that's the reason of Section 1 to 5 divided upon.

Consider Section 1: when current is injected, it is reasonable that the low-resistance PPA segment with less impendence enjoys larger current and lase first as long as the quantum well region in the SG segment becomes transparent, judging from the low SMSR of the spectrum mentioned above. The lasing PPA segment is a diode in conductive state, yet the SG segment is still cut off, without any gain but only intrinsic loss. This is making a weaker DFB effect, inducing a lower SMSR. This can be solved by enlarging the length of PPA segment with more periods to offer stronger optical feedback in actual uses (in this device PPA segment is only 1 mm in length with a limited number

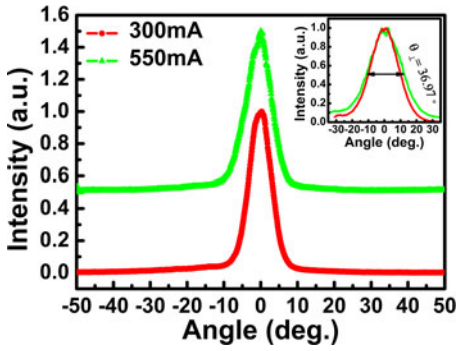

Fig. 10. Measured far-field patterns (FFPs) of slow axis in CW mode. The inset shows FFP of fast axis.

160 periods, longer length with more number of periods will offer better feedback to increase the SMSR for practical applications). When current rises, PPA segment lases and causes carrier density distribution changes, leading to gain peak changes and making the tuning effect.

Consider Section 2: when current further rises and voltage comes up, as the SMSR increase to over 30 dB, the SG segment is taking a part of gain, even though not be able to overcome the intrinsic loss to lase thus still cut off because the current of PPA segment is still below the threshold current for the single PPA segment (150 mA), but is able to offer feedback to increase SMSR. This tends to stabilize the wavelength and prevent the spectrum from further red shift, making a stable region at around 300 mA to 340 mA.

Consider Section 3: This is a changing section. As the resistance ratio of SG segment versus PPA segment is 1.2 and two segments are electrically parallel connected, when current continues to rise to 340 mA, the current in the SG segment is about 154 mA, meaning the SG segment is becoming conductive as the threshold current for the single SG is about 150 mA as shown in Fig. 7.The inset of the Fig. 3 cloud also clarify this change by the small change of dV/dI vs current characteristic, inducing a large current redistribution. Current in PPA segment reduced dramatically, making this segment cooler again. When current in SG segment is still week, PPA segment still dominates the lasing spectrum. The larger conductivity of the SG segment is, the less current injects in PPA segment. Under a 20 °C water cooled circumstance, the temperature of PPA segment drops along. That's causing the tuning effect of a blue shift lasing spectrum.

Consider Section 4: Even though the SG segment is no longer shut off, it still have 1.2 times higher resistance than the PPA segment, taking less current than the later thanks to etched high doping/ (high conductive) cap layer. The control of the current distribution by the resistance ratio in the two segments could cause the carrier density distribution, leading to the gain peak changes. As the PPA segment could be gain saturation when current increase larger than about 200 mA as shown in Fig. 7, leading to the SG segment would provide the feedback effect. Hence, in this case with the resistance ration of 1.2, when the current increase to 380 mA, the current for PPA segment is about 206 mA, meaning the wavelength modulation provided only by the SG segment to gain a stable spectrum. Hence, the emission wavelength can be designed by the resistance ratio in the two segments through the number or duty of grating period. Since SG segment has better optical feedback due to larger gain difference calculated above, it's becoming the master oscillator, and PPA segment which takes most of the current injection, works as a slave power amplifier, leading to the feedback effect being reduced a little to cause the decrease of SMSR as shown in the inset of Fig. 5. The current in SG component grows so slowly to maintain a stable spectrum over a large current region from 380 mA to 520 mA, with high SMSR (∼30 dB).

Consider Section 5: when current continues to rise, the PPA segment reaches gain saturation, and SG segment has to overtake the continuously rising current, which is rising its temperature and shows the tuning effect again.

Fig. 10 shows the measured far-field pattern in CW mode. The beam divergence of the slow axis and fast axis at full width at half maximum (FWHM) is less than 7.2° and 36.97° respectively over

the entire tuning range. The main lobe is nearly Gaussian distributed without degraded and there are no evidence that any higher order transverse mode lasing up to the high output power at single longitudinal mode operation. The value of the beam propagation factors M^2 in slow axis is only 1.54, indicating a single transverse mode lasing. High beam quality with single transverse mode is suitable for beam shaping and fiber coupling.

4. Conclusion

We have presented a low-cost practical regrowth-free two-segment gain-coupled distributed feedback (DFB) laser, possessing both wavelength-tunable and wavelength stabilization characteristics simultaneously for the first time among reported gain-coupled DFB lasers, to our best knowledge. The device monolithically integrated a low gain contrast segment with only periodic surface metal p-contact, and a high gain contrast segment with etched grooves of the same period forming gain-coupled DFB lasers. Thanks to gain-coupled DFB effect, single longitudinal mode with tuning range beyond 5 nm simply by injection current is achieved, which is much larger than the existing structures ($\sim$1 nm). And stable wavelength at 973.80 $\pm$ 0.04 nm is obtained at a large current range from 380 mA to 520 mA, which may be applied in pumping sources and arrays for solid-state lasers and fiber lasers. The single electrode configuration can maintain a long-term stable operation and avoid complex separate top contacts (three-terminal configuration) fabrication. At current larger than 320 mA, SMSR reached over 30 dB with linewidth smaller than 80 pm. Our uncoated device has a CW power reached 159 mW/facet at single mode operation. Considering both facets all together, it is at the same power level of index-coupled DFB lasers. Surface grooves and 4-μm-width ridge were patterned simultaneously by merely i-line lithography. With a simple and robust technique, it provides a novel method for low-cost, monolithically integrated wavelength-tunable and wavelength stabilization DFB lasers, meeting requirement of either/both wavelength tunable or/and wavelength stabilization characteristics. Future work will be concentrated on making devices at wavelengths like 1550 nm for widespread applications in optical communication.

Reference

[1] A. R. Nehrir, K. S. Repasky, and J. L. Carlsten, "Eye-safe diode-laser-based micropulse differential absorption lidar (DIAL) for water vapor profiling in the lower troposphere," *J. Atmos. Ocean. Technol.*, vol. 28, no. 2, pp. 131–147, 2011.

[2] H. Jeon, J. M. Verdiell, M. Ziari, and A. Mathur, "High-power low-divergence semiconductor lasers for GaAs-based 980-nm and InP-based 1550-nm applications," *IEEE J. Sel. Top. Quantum Electron.*, vol. 3, no. 6, pp. 1344–1350, Dec. 1998.

[3] J. W. Zimmerman, R. K. Price, U. Reddy, N. L. Dias, and J. J. Coleman, "Narrow linewidth surface-etched DBR lasers: Fundamental design aspects and applications," *IEEE J. Sel. Top. Quantum Electron.*, vol. 19, no. 4, Jul.–Aug. 2013, Art. no. 1503712.

[4] E. C. Burrows and K. Y. Liou, "High resolution laser LIDAR utilising two-section distributed feedback semiconductor laser as a coherent source," *Electron. Lett.*, vol. 26, no. 9, pp. 577–579, 1990.

[5] I. Kim *et al.*, "Broadly tunable vertical-coupler filtered tensile-strained InGaAs/InGaAsP multiple quantum well laser," *Appl. Phys. Lett.*, vol. 64, no. 21, pp. 2764–2766, 1994.

[6] H. Ishii, Y. Tohmori, M. Yamamoto, T. Tamamura, and Y. Yoshikuni, "Modified multiple-phase-shift superstructure-grating DBR lasers for broad wavelength tuning," *IEEE Photon.Technol. Lett.*, vol. 5, no. 11, pp. 1683–1690, Jul. 1994.

[7] M. Oberg, S. Nilsson, K. Streubel, and J. Wallin, "74 nm wavelength tuning range of an InGaAsP/InP vertical grating assisted codirectional coupler laser with rear sampled grating reflector," *IEEE Photon. Technol. Lett.*, vol. 5, no. 7, pp. 735–737, Jul. 1993.

[8] K. Kikuchi and H. Tomofuji, "Analysis of oscillation characteristics of separated-electrode DFB laser diodes," *IEEE J. Quantum Electron.*, vol. 26, no. 10, pp. 1717–1727, Oct. 1990.

[9] M. Nawrocka *et al.*, "Widely tunable six-section semiconductor laser based on etched slots," *Opt. Exp.*, vol. 22, no. 16, p. 18949–18957, 2014.

[10] R. J. Guo *et al.*, "Multisection DFB tunable laser based on REC technique and tuning by injection current," *IEEE Photon. J.*, vol. 8, no. 4, Aug. 2016, Art. no. 1503007.

[11] J. Hong, H. Kim, and T. Makino, "Enhanced wavelength tuning range in two-section complex-coupled DFB lasers by alternating gain and loss coupling," *J. Lightw. Technol.*, vol. 16, no. 7, pp. 1323–1328, Jul. 1998.

[12] J. Fricke *et al.*, "Properties and fabrication of high-order Bragg gratings for wavelength stabilization of diode lasers," *Semicond. Sci. Technol.*, vol. 27, no. 27, 2012, Art. no. 055009.

[13] D. T. Nichols, J. Lopata, W. S. Hobson, and P. F. Sciortino, "DFB and DBR lasers emitting at 980 nm," *Electron. Lett.*, vol. 29, no. 23, pp. 2035–2037, 1993.
[14] R. M. Lammert, J. E. Ungar, S. W. Oh, and H. Qi, "980 nm high power, high slope efficiency distributed feedback lasers with nonabsorbing mirrors," *Electron. Lett.*, vol. 34, no. 17, pp. 1663–1664, 1998.
[15] Y. Park, S. T. Lee, and C. J. Chae, "A novel wavelength stabilization scheme using a fiber grating for WDM transmission," *IEEE Photon. Technol. Lett.*, vol. 10, no. 10, pp. 1446–1448, Oct. 1998.
[16] B. L. Volodin, S. V. Dolgy, E. D. Melnik, E. Downs, J. Shaw, and V. S. Ban, "Wavelength stabilization and spectrum narrowing of high-power multimode laser diodes and arrays by use of volume Bragg gratings," *Opt. Lett.*, vol. 29, no. 16, pp. 1891–1893, 2004.
[17] A. J. Keating and A. J. Lowery, "Wavelength stabilization in packet-switched WDM networks," *J. Lightw. Technol.*, vol. 15, no. 1, pp. 76–85, Jan. 1997.
[18] D. Kais, B. Abdessamad, Z. Jessica, H. Karin, and T. J. Hall, "Narrow linewidth two-electrode 1560 nm laterally coupled distributed feedback lasers with third-order surface etched gratings," *Opt. Exp.*, vol. 22, no. 16, pp. 19087–19097, 2014.
[19] Y. Yoshikuni and G. Motosugi, "Multielectrode distributed feedback laser for pure frequency modulation and chirping suppressed amplitude modulation," *J. Lightw. Technol.*, vol. 5, no. 4, pp. 516–522, Apr. 1987.
[20] Y. Yoshikuni, K. Oe, G. Motosugi, and T. Matsuoka, "Broad wavelength tuning under single-mode oscillation with a multi-electrode distributed feedback laser," *Electron. Lett.*, vol. 22, no. 22, pp. 1153–1154, 1986.
[21] Z. J. Fang and S. Wang, "Longitudinal mode behavior and tunability of separately pumped (GaAl)As lasers," *Appl. Phys. Lett.*, vol. 44, no. 1, pp. 13–15, 1984.
[22] H. Kogelnik and C. V. Shank, "Coupled-wave theory of distributed feedback lasers," *J. Appl. Phys.*, vol. 43, no. 5, pp. 2327–2335, 1972.
[23] Y. Luo, Y. Nakano, K. Tada, T. Inoue, H. Hosomatsu, and H. Iwaoka, "Purely gain-coupled distributed feedback semiconducutor lasers," *Appl. Phys. Lett.*, vol. 56, no. 17, pp. 1620–1622, Apr. 1990.
[24] N. Susa, "Fluctuations of the laser characteristics and the effect of the index-coupling component in the gain-coupled DFB laser," *IEEE J. Quantum Electron.*, vol. 33, no. 12, pp. 2255–2265, Dec. 1997.
[25] S. T. Kim and B. G. Kim, "Analysis of single-mode yields above threshold for complex-coupled distributed feedback lasers with asymmetric facet reflectivities," *J. Opt. Soc. Amer. B.*, vol. 22, no. 5, pp. 1010–1015, May 2005.
[26] A. J. IEEE Photonics Technology LettersLowery and D. Novak, "Performance comparison of gain-coupled and index-coupled DFB semiconductor lasers," *IEEE J. Quantum Electron.*, vol. 30, no. 9, pp. 2051–2063, Sep. 1994.
[27] T. P. Nguyen *et al.*, "Optimization of 780 nm DFB diode lasers for high-power narrow linewidth emission," *Appl. Phys. B*, vol. 108, no. 4, pp. 767–771, 2012.
[28] S. Spiebberger, M. Schiemangk, A. Wicht, H. Wenzel, O. Brox, and G. Erbert, "Narrow linewidth DFB lasers emitting near a wavelength of 1064 nm," *J. Lightw. Technol.*, vol. 28, no. 17, pp. 2611–2616, Sep. 2010.
[29] B. W. Hakki, "Carrier and gain spatial profiles in GaAs stripe geometry lasers," *J. Appl. Phys.*, vol. 44, no. 11, pp. 5021–5028, 1973.
[30] H. Wenzel, J. Fricke, J. Decker, P. Crump, and G. Erbert, "High-power distributed feedback lasers with surface gratings: Theory and experiment," *IEEE J. Sel. Top. Quantum Electron.*, vol. 21, no. 6, pp. 352–358, Nov./Dec. 2015.
[31] J. Decker *et al.*, "25-W monolithic spectrally stabilized 975-nm minibars for dense spectral beam combining," *IEEE Photon. Technol. Lett.*, vol. 27, no. 15, pp. 1675–1678, Aug. 2015.
[32] S. L. Chuang, *Physics of Photonic Devices.* Berlin, Germany: Wiley, 2009.
[33] Y. Shi, S. Li, R. Guo, R. Liu, Y. Zhou, and X. Chen, "A novel concavely apodized DFB semiconductor laser using common holographic exposure," *Opt. Exp.*, vol. 21, no. 13, pp. 16022–16028, 2013.
[34] J. Li *et al.*, "Experimental demonstration of distributed feedback semiconductor lasers based on reconstruction-equivalent-chirp technology," *Opt. Exp.*, vol. 17, no. 7, pp. 5240–5, 2009.
[35] J. Decker, P. Crump, J. Fricke, A. Maassdorf, G. Erbert, and G. Trankle, "Narrow stripe broad area lasers with high order distributed feedback surface gratings," *IEEE Photon. Technol. Lett.*, vol. 26, no. 8, pp. 829–832, Apr. 2014.
[36] T. N. Vu, A. Klehr, B. Sumpf, H. Wenzel, G. Erbert, and G. Tränkle, "Tunable 975 nm nanosecond diode-laser-based master-oscillator power-amplifier system with 16.3 W peak power and narrow spectral linewidth below 10 pm," *Opt. Lett.*, vol. 39, no. 17, pp. 5138–5141, 2014.